Original Article

Microbial Biosystems 10(2) (2025) 2025.342997
10.21608/mb.2025.342997.1217

Contents lists available at Egyptian Knowledge Bank
Microbial Biosystems
Journal homepage: http://mb.journals.ekb.eg/

Investigation of the effects of chitosan-zinc and colistin-chitosan nanoparticles on *bap* genes in the biofilm formation of *Acinetobacter baumannii*

Yousif Salih Abdul Jabbar[1], Mais Emad Ahmed[2*], Umut Gazi[1]

[1] *Department of Medical Microbiology and Clinical Microbiology, Faculty of Medicine, Near East University, Nicosia 99138, Cyprus.*
2 *Department of Biology, College of Science, University of Baghdad, Baghdad, Iraq.*

ARTICLE INFO

Article history
Received 10 December 2024
Received revised 25 December 2024
Accepted 04 April 2025
Available online 01 June 2025

Corresponding Editors
Mekky, A. E.
Abdel-Azeem, A. M.

Keywords
Antimicrobial resistance,
biofilm inhibition,
chitosan nanoparticles,
gene expression,
zinc oxide.

ABSTRACT

Acinetobacter baumannii is a major cause of skin infections, largely due to biofilm formation and antibiotic resistance. This study evaluates the antimicrobial potential of Chitosan-Zinc Oxide Nanoparticles (CS-ZnO-NPs) and a colistin-chitosan combination (Col-CS-NPs) against biofilm-associated, multidrug-resistant *A. baumannii*. CS-ZnO-NPs were synthesized using chitosan biomass and characterized via FTIR, UV-visible spectrometry, X-ray diffraction (XRD), and microscopy (TEM, FESEM, AFM). XRD confirmed a hexagonal structure, and AFM showed particle sizes of 34–65 nm. UV absorption at 235 nm reflected optical properties, while FESEM verified morphology. The microdilution method established the nanoparticles' minimum inhibitory concentration (MIC), demonstrating antifungal activity and synergistic inhibition of fungal strains. PCR confirmed the *bap* gene in most isolates, and RT-PCR showed variation in gene expression. CS-ZnO-NP treatment significantly downregulated *bap* expression in strong biofilm producers. Cytotoxicity assays on A375 cells revealed IC50 values of 2.5 µg/mL for CS-ZnO-NPs and 1.5 µg/mL for Col-CS-NPs. CS-ZnO-NPs induced higher cell mortality. Combining CS-ZnO-NPs with agents like Extr-DA-NPs and MFX0.5SF inhibited biofilm formation and reduced bacterial fouling within 24–48 hours at 37°C. Real-time PCR confirmed decreased *bap* expression post-treatment. These results demonstrate a dose-dependent bactericidal effect of CS-ZnO-NPs, indicating strong therapeutic potential. Further research is warranted to explore their clinical applications and safety in managing multidrug-resistant infections.

Published by Arab Society for Fungal Conservation

Introduction

Acinetobacter baumannii (*A. baumannii*) possesses unique characteristics that enable it to compromise the body's immune system, making it a significant contributor to hospital-acquired infections. This organism can colonize living tissues and inanimate surfaces and possesses remarkable adaptability in surviving antibiotic exposure. Its success in resisting antibiotics is facilitated by various resistance mechanisms, which may be either transmissible (passed between organisms) or intrinsic (non-transmissible and inherent to the organism) (Ahmed et al., 2024).

Acinetobacter baumannii has emerged as a critical public health concern due to its ability to cause severe infections in hospitalized patients, especially those with weakened immune systems. Its notable resistance to

* *Corresponding author Email address*mais.emad@sc.uobaghdad.edu.iq (Mais Emad Ahmed)

various antibiotics makes it a formidable pathogen. The exploration of nanoparticle-based solutions, such as zinc oxide and chitosan nanoparticles, presents a promising frontier in combating this bacterium, offering potential breakthroughs in disrupting its biofilm formation and enhancing antibacterial efficacy.

Biofilm formation, a structured community of bacterial cells encased within a self-produced extracellular matrix, is a key factor contributing to the infectious capability of *Acinetobacter baumannii* by enhancing its resistance to environmental stresses and antimicrobial treatments. This study investigates the influence of stored *Acinetobacter baumannii* in ventilator-associated pneumonia (VAP) through biofilm formation (Salman & Ahmed, 2024).

Biological biofilms are structured communities of certain bacteria encased in polysaccharides, proteins, lipids, and extracellular DNA matrix. The complex communication systems among the biofilm community empower the infections to grow hale and hearty enough to oppose various challenges, including medications and the host's immune responses (Fawzi & Ahmed, 2024).

The phenotype of *A. baumannii* includes a variety of diseases caused not only by bacterial virulence factors but also by food acquisition, community interactions, and the genetic modulation of virulence. The interactions within the quorum-sensing community—a cell-to-cell communication system regulated by signaling molecules that coordinate group behaviors—are crucial for the survival of the *A. baumannii* population. Understanding these interactions, which regulate biofilm formation, virulence, and antibiotic resistance, is essential for the survival and spread of *A. baumannii*." (Chukamnerd et al., 2024).

Researchers are actively working to develop new antibiotic treatments that target biofilm-forming bacteria and tackle the increasing issue of multidrug resistance (MDR) in a rapidly changing environment. (Muunim et al., 2019).

The green synthesis of metal oxide nanoparticles is gaining significant attention due to its eco-friendly approach and potential applications in various fields, including biotechnology and healthcare. (Abdel-Azeem et al. 2020, Emad & Salama 2020, Srivastava et al. 2021, Gezaf et al. 2022, Mossa et al. 2024, Abd-Elhameed et al. 2024, Abdulameer et al. 2024, Alnagar et al. 2025, Salah et al. 2025, Hussein et al. 2025). ZnO nanoparticles derived from plants are a common medium for organic synthesis and can effectively kill several types of bacteria. Their solidity is a combination of their physical shapes, disk-like morphology, high aspect ratio, and small scale, which makes them great candidates for the adhesion of bacterial cells (Seddiq et al., 2023).

Zinc oxide, a naturally occurring metal oxide, is the most important. It has physiological uses that encompass both anti-inflammatory and antibacterial effects. Several studies have proved that the quorum sensing system is one. Such a possibility would be established if the quorum sensing system were inhibited by antibacterial agents that would prevent biofilm formation afterward (Mahdi et al., 2024).

Chitosan is known to be a good choice of organic polymers for several reasons. For one, it has functional groups that can bind metal ions, which, in turn, makes it a beautiful material for the development of Nano-hybrids. In addition, the chitosan (CS) copolymer the primary characteristic of which is non-toxic, biocompatible, and biodegradable, which allows it to be the best in its class in the field of environmentally friendly polymers and the medical area (Jaber et al., 2022).

Chitosan nanoparticle (CNPs) production enables the realization of specific nano-scale features such as small size, surface modification, and quantum size effects. CNPs have immense potential for medical applications like drug delivery, genetic therapy, tissue engineering, and the treatment of various diseases. One of the paper's main objectives is to deal with the reason behind using various synthesis methods and determine their effects on the structural and related properties of CNPs (Divya & Jisha, 2018).

As far as polymyxins are concerned, the fact that colistin comes with the risk of cellular toxicity is well-known, and it is a significant concern. The potential application of gold nanoparticles (AuNPs) for reducing the toxic effects of colistin has been studied. The present research sought to determine the antimicrobial activity of colistin in combination with chitosan-capped gold nanoparticles (CS-AuNPs) and their formulation for aerosolizing the product to the deep lung using metered-dose inhalers (MDIs).

The prepared samples of Azithromycin-NPs underwent studies using elemental analysis, nuclear magnetic resonance, and Fourier-transform infrared spectroscopy. Drug release profiles were also analyzed to identify the most suitable release kinetic model (Changsan et al., 2024).

This study evaluated the anti-biofilm properties of environmentally friendly nanoparticles, chitosan-synthesized-zinc oxide (CS-ZnO NPs), against the causative factor of biofilm formation *Acinetobacter baumannii*. Similarly, because of the specificity of chitosan, which was discussed before, researchers should focus on producing CS-ZnO nanoparticles and then check their cytotoxicity and antibacterial efficacy against multidrug-resistant bacterial strains. Furthermore, sulfate and chitosan incorporated with nanomaterials were

compatible in various cross-linking and infused with CS-ZnO NPs in different amounts.

The chemical compositions of the hydrogels and CS-ZnO NP biocomposites were investigated via the following analysis techniques: elemental analysis, FTIR, XRD, EDS, and SEM. In addition to these, the study examined the use of chitosan and CS-ZnO NP biocomposites on the bacteria, and then, from those, speculating on the cytotoxicity of these materials is the central point of our interest.

This research is significant in addressing the growing threat of multidrug-resistant *Acinetobacter baumannii*, a leading cause of hospital-acquired infections. By focusing on environmentally friendly nanoparticles, this study aims to provide innovative approaches to combat antibiotic-resistant bacteria and improve the effectiveness of medical treatments. The findings could have profound implications for healthcare, including developing advanced therapies to manage persistent infections.

Materials and Methods

Sample collection

One hundred clinical samples were collected from wound swabs from patients at the resident hospital in AL Yarmouk Teaching Hospital. The samples were cultured immediately after collection for diagnostic purposes. The samples were then identified primarily by culturing on MacConkey at 37C for 24 h. and confirmed by the VITEC 2 system (Hassoon et al., 2019).

Conforming to the guidelines published by the Clinical & Laboratory Standards Institute: CLSI Guidelines 2023, susceptibility testing occurs on Mueller Hinton agar plates via the disk method (Rasheed et al., 2023).

Preparation of CS-ZnO NPs

The zinc oxide nanoparticles (ZnO NPs) were synthesized using a rapid co-precipitation method at ambient temperature (Hassan et al., 2022). Initially, 0.5 mL of zinc acetate dehydrate solution was prepared at room temperature and adjusted to a pH of 7 using a 0.5 mL sodium hydroxide solution, forming a ZnO NP suspension. The suspended particles were cleaned through repeated washing with deionized water while under magnetic stirring to remove residual zinc acetate and other impurities (Dil et al., 2020).

To prepare the chitosan coating, 2 grams of powdered chitosan were dissolved in 100% acetic acid and stirred magnetically for 2 hours to achieve a homogeneous solution. Following this, 0.5 mL of sodium hydroxide solution was added to the chitosan solution under constant stirring for 10 minutes to facilitate gelation.

The prepared (ZnO NPs) suspension was gradually introduced into the chitosan solution under continuous stirring to integrate ZnO nanoparticles with chitosan. This allowed the ZnO particles to be uniformly dispersed and embedded within the chitosan matrix. This mixture was stirred further to ensure a consistent blend, resulting in a light milky suspension designated as CS-ZnO NPs.

To remove excess zinc acetate, sodium hydroxide, and other contaminants, the final suspension was subjected to multiple washings with deionized water and ethanol before being dried in a microwave oven at 120°C for 15 minutes. The resulting CS-ZnO NPs exhibited uniform structure and were suitable for subsequent characterization and antibacterial evaluation.

Preparation of Col-CS-NPs

This study aims to develop chitosan-coated colistin nanoliposomes to enhance colistin sulfate's stability and antimicrobial activity using chitosan with a medium molecular weight of 190,000 Da. A previously reported protocol was modified to synthesize Col-CS-NPs (Fuster et al., 2020).

The first step in preparing the chitosan solution involved dissolving 0.5 g of powdered chitosan in 50 mL of a 1% acetic acid solution. The solution was thoroughly mixed and left under continuous agitation at room temperature (25–30°C) for 24 hours to achieve complete dissolution and uniformity.

To synthesize Col-CS nanoparticles (Col-CS-NPs), 10 mg/mL of colistin sulfate and 1 mL of glutaraldehyde (25% aqueous solution) were slowly introduced into the prepared chitosan solution under magnetic stirring.

The addition of glutaraldehyde acted as a crosslinking agent, facilitating the formation of a stable chitosan nanoparticle structure. This process was carried out under sterile conditions to maintain the formulation's antimicrobial efficacy.

After synthesis, the Col-CS -NPs were dried using microwave oven radiation to remove solvents and achieve a stable nanoparticle form. The final product, Col-CS-NPs, was then prepared for further characterization and evaluation of its physicochemical properties and antimicrobial activity (Mahdi et al., 2024).

Characterization of CS-ZnO NPs and Col-CS nanoparticles

Understanding the distinctive features of nanoparticles requires characterization. The shapes and sizes of the nanoparticles were identified using the following techniques: Field Emission Scanning Electron Microscopy (FE-SEM) was employed to graphically represent and evaluate the surface morphology, particle size distribution, shape of the particle or crystal, agglomeration of nanoparticles, surface functionalization, and single-particle evaluations.

UV-visible (UV-DRS) is used to investigate the optical properties of the materials. In contrast, atomic force microscopy (AFM) is used to determine the diameter and height of NPs in 3D vision. (XRD) is a method used in materials science to identify a material's crystallographic structure.

Functional groups of prepared nanostructures in the range of 4000–400 nm were examined by Fourier-transform infrared spectroscopy (FT-IR, RX I, PerkinElmer, Inc., USA) at a resolution of 4 cm1 and Zeta Potential (ZP) and energy dispersive X-ray (EDX).

The minimal inhibitory concentration (MIC) determination

The minimal inhibitory concentration (MIC) of Col-CS and CS-ZnO nanoparticles that inhibit bacterial growth was Fig.d using the Eppendorf tubes and the microdilution broth method. A microbial inoculum was prepared in Mueller Hinton Broth (MHB), and its concentration was adjusted to 100 CFU/µl. CS-ZnO nanoparticles were serially diluted twice in six tubes with concentrations of 1000, 500, 250, 125, and 64 µg/µl, and the diluent was MHB.

The tubes were incubated at 37°C for 24 hours. The results were evaluated based on bacterial growth observed in/by each tube and by which the sub-MIC levels could be determined (Romi & Ahmed, 2024).

Antifungal properties of CS-ZnO NPs and Col-CS NPs

Natural product-based metallic nanoparticles offer a variety of bioactivities, including antibacterial properties. The microorganism's resistance to different medications and distinct cell membrane composition limits its bioactivity. Mueller-Hinton agar was used for the agar-well diffusion assay.

Using sterile inoculating loops or swabs, test isolates of Staphylococcus species and a few harmful fungi were deposited onto Muller-Hinton agar plates. Five 5 mm wells were created using a sterile cork borer, and 80 µl of various concentrations—which vary depending on the microdilution technique below—were then inserted.

The inhibition zones were evaluated the following day after being incubated for 24 hours at 37 °C. Additionally, the pathogenic fungal isolates from skin infection (*Candida albicans, Candida guilliermondii, Candida ferric)* that were used were obtained, identified, and isolated from the Iraqi University College of Medicine. Lastly, confirmation identification was done using the VITEK 2 system (Ahmed & Kadhim, 2018).

Cytotoxicity assay of CS-ZnO NPs and Col-CS NPs

The MTT test was employed to evaluate the cell viability for various doses of CS-ZnO NPs and Col-CS NPs (1, 1.5, 2, 2.5, and 3µg/ml) against malignant cells (A375 cells) and typical fibroblast cells (WRL68 cells) (Rashid et al., 2022).

Estimation of biofilm formation

Bacteria grown in broth were utilized to produce the 1:100 diluted biofilm inoculums, which were subsequently transferred to the 200 l well. The broth was used in the negative control wells (200 l of BHI supplemented with 1% glucose per well). Every strain completed three different tests (Faiq & Ahmed, 2024).

Under static conditions, the inoculated plate was covered with a lid and incubated aerobically for 24–30 hours at 35–37 °C. Numerous bacteria MDR Multidrug resistance (Y1-Y2).

Using a microtiter-plate reader (GloMax/ Promega-USA), each well's optical density (OD) was measured at 630 nm. Three standard deviations (SD) above the median OD of the negative control, or ODc, is the cut-off value for the adverse control. Average OD for the negative control plus (3× SD of the negative control) yields ODc.

Evaluation of bap gene by PCR

Bacterial genomic DNA was extracted from all isolates according to the kit protocol; the *bap gene* was detected by PCR using specific primers (Table 1). Electrophoresis was performed on 1.5% agarose gels and was visualized by an ultraviolet gel documentation system (BioRad, USA). *Acinetobacter baumannii* was used as a positive control.

Bap gene detection

This was done by using the polymerase chain reaction (PCR) technique. The tested gene was amplified using a primer and conventional PCR. The sequence is from (Bahador et al., 2015). The PCR amplifications were performed with 20µl volumes that contained 10µl of GoTaq Green Master Mix (2X), 1µl of primer (10 pmol), 6µl of nuclease-free water, and 2µl of template DNA.

Thermo Fisher Scientific and USA's PCR Express (thermal cycler) cycle the PCR according to the following temperature program: Denaturation was started for five minutes at 95°C. There were then thirty cycles of denaturation at 95°C for thirty seconds, annealing at 50, 55, and 60°C for thirty seconds, and extension at 72°C for thirty seconds.

The last extension step was run for seven minutes at 72°C, and then the reactions were stopped with a ten-minute incubation at 10°C. Table (1*)* indicated that a *Bap gene* primer was utilized.

Table 1 Forward and reverse primer sequences for the *Bap* gene and its associated housekeeping genes used for normalization in PCR analysis according to Azizi et al. (2016).

Primer Name	Sequence 5`-3`	Annealing Temp. (°C)	Product size (bp)
Bap-F	TGCTGACAGTGACGTAGAACCACA	60	184
Bap-R	TGCAACTAGTGGAATAGCAGCCCA	60	184
Acba-16s -F	CCTACCTGTTGGTCTTCGACCCG	58	279
Acba-16s -R	GCTGATGTTGTCGTGGGTGAGG	58	279

Detection of bap gene expression

The analysis and Calculation of gene expression levels of one or more genes depend on RNA concentration after conversion to cDNA. This was done using the Real-Time PCR Technique to estimate the expression of genes treated with CS-ZnO NPs and Col-CS NPs. Table (2) shows the reaction setup.

According to the program that follows: RT. Enzyme Activation First initiated a 15-minute cycle at 37°C, followed by a 5-minute initial denaturation cycle at 95°C. The subsequent forty cycles included twenty seconds of denaturation at 95°C, twenty seconds of annealing at 58 and 60°C, and twenty seconds of extension at 72°C.

Table 2. Reaction setup components and thermal cycling conditions used for PCR amplification of target genes.

Master mix components	Stock	Unit	Final	Unit	Volume 1 sample
qPCR Master Mix	2	X	1	X	5
RT mix	50	X	1	X	0.25
MgCl2					0.25
Forward primer	10	µM	0.5	µM	0.5
Reverse primer	10	µM	0.5	µM	0.5
Nuclease Free Water					2.5
RNA		ng/µl		ng/µl	1
Total volume					10
Aliquot per single rxn	9µl of Master mix per tube and add 1µl of Template				

Real-time-quantification PCR (RT-qPCR) protocol

Real-time quantification of cDNA was carried out on the GoTaq® 1-Step RT-qPCR System (Promega, USA) using the qPCR master mix. RT-PCR was used to investigate the expression levels of the ***bap gene***. The results were normalized using the Acba-16s, considered a housekeeping gene, to assess the *bap* gene's expression.

Primers of these genes (table 1) were provided in a lyophilized form and dissolved in sterile nuclease-free water to give a final concentration of 100 pmol/µl. Afterward, they were stored in a deep freezer until used in qPCR. The reaction mixture is summarized in Table (2), and the qRT-PCR program is outlined in Table (3).

Table 3. Reverse transcription PCR (RT-PCR) program parameters, including temperature and duration for each cycling step.

Steps	°C	Time m: s	Cycle
RT. Enzyme Activation	37	15:00	1
Initial Denaturation	95	05:00	
Denaturation	95	00:20	
Annealing	58, 60	00:20	40
Extension	72	00:20	

The difference in cycle thresholds (Ct) and fold changes between the treated groups and the calibrators for each gene were evaluated. The rpo values were used to normalize the data using the Livak formula (Passat, 2016).

Results

Isolation and identification

A total of sixty-four Isolates were confirmed as *A. baumannii*; the VITEK 2 system carried out the conformation, considered a reliable identification technique, displayed pale, round colonies on MacConkey agar, and was a non-lactose fermenter as shown in figure1.

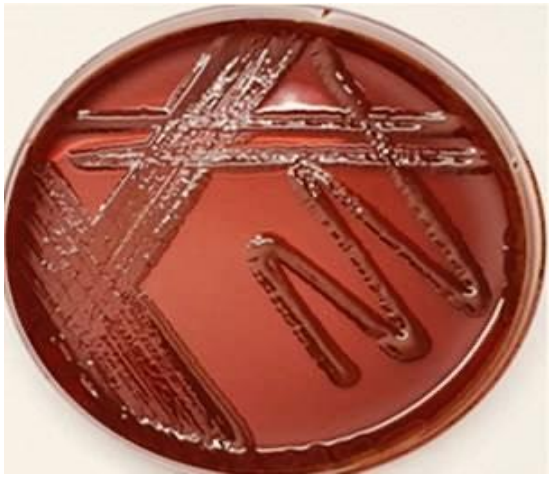

Fig 1. *Acinetobacter baumannii* isolates cultured on MacConkey agar, showing characteristic non-lactose fermenting colonies.

Antibiotic susceptibility test

According to the latest investigation, clinical isolates of *A. baumannii* displayed substantial resistance to most antibiotics used to evaluate. In particular, isolates of *A. baumannii* illustrated 100% resistance to the following kinds of antibiotics: The following percentages among patients showed resistance: 96.7% for amikacin, 76.7% overall imipenem and meropenem, and 66.7% for levofloxacin as seen in figure 2.

Synthesis of CS-ZnO NPs and Col-CS-NP:

The prepared Chitosan/ZnO nanoparticles in powder form at 120 °C were then characterized, and the formation of a white precipitate indicated the formation of nanoparticles. After centrifugation, the precipitate appeared white. After drying with the microwave, we obtained a shiny white powder, as shown in figure 3a.

The present study investigates the impact of Zn and CS combinations on the antibacterial activity of coated textile surfaces. This first study describes a one-step magnetic starrier approach for forming organometallic nanocomposites on fabrics. The Col-CS-NP solution's color and clarity were assessed visually, and the colloidal characteristics were verified using the Tyndall effect (Fig. 3b).

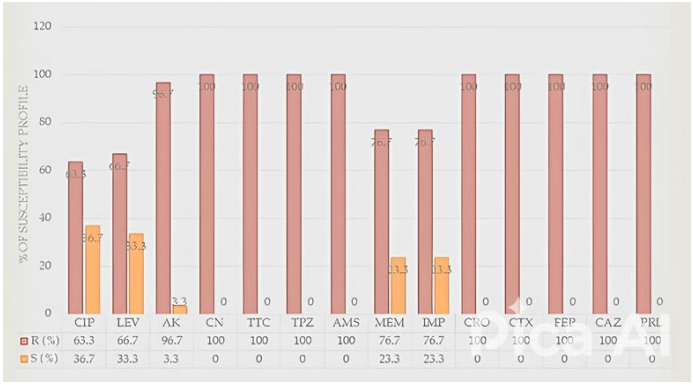

Fig 2. Antibiotic susceptibility profile of *Acinetobacter baumannii* isolates, illustrating resistance and sensitivity patterns to various antimicrobial agents.

Characterization of CS-ZnO NPs and Col-CS-NP

UV–Vis Spectral Analysis and Zeta Potential Analysis

The production of CS-ZnO NPs has been confirmed through UV-visible spectroscopy. For this experiment, the sample was submerged in deionized water. Data revealed the presence of newly synthesized CS-ZnO NPs, with a characteristic absorption peak at 235 nm, indicating the excitation of nanoparticles from the ground state to the excited state and demonstrating the uniformity of particle sizes in the nanoscale range (Fig. 4a, b).

While the Col-CS NPs showed a slightly larger absorption peak at 216 nm, signifying an increase in particle size after conjugation, their particle size distribution remained within a narrow range (200 nm—400 nm). This is critical for ensuring consistent optical and antimicrobial properties for medical applications.

Zeta potential indicates particle stability in colloidal systems, with higher absolute values signifying stronger repulsion and stability. Lower values near zero suggest weak repulsion and potential aggregation.

CS-ZnO nanoparticles display a zeta potential close to 0 mV, indicating lower colloidal stability and a higher tendency to aggregate (Fig. 5a). In contrast, Col-CS nanoparticles exhibit a zeta potential of approximately -50 mV, reflecting high stability due to strong negative surface charges (Fig. 5b).

Atomic Force Microscopy (AFM) analysis

AFM analysis of CS-ZnO NPs was performed with CSPM (Contact Scanning Probe Microscopy: A Technique for Imaging and Measuring Surface Properties using a nanoscale tip in direct contact with the sample) to identify and characterize nanoparticle distributions. The chitosan-zinc oxide (ZnO) nanocomposite's microstructure was investigated utilizing atomic force microscopy (AFM).

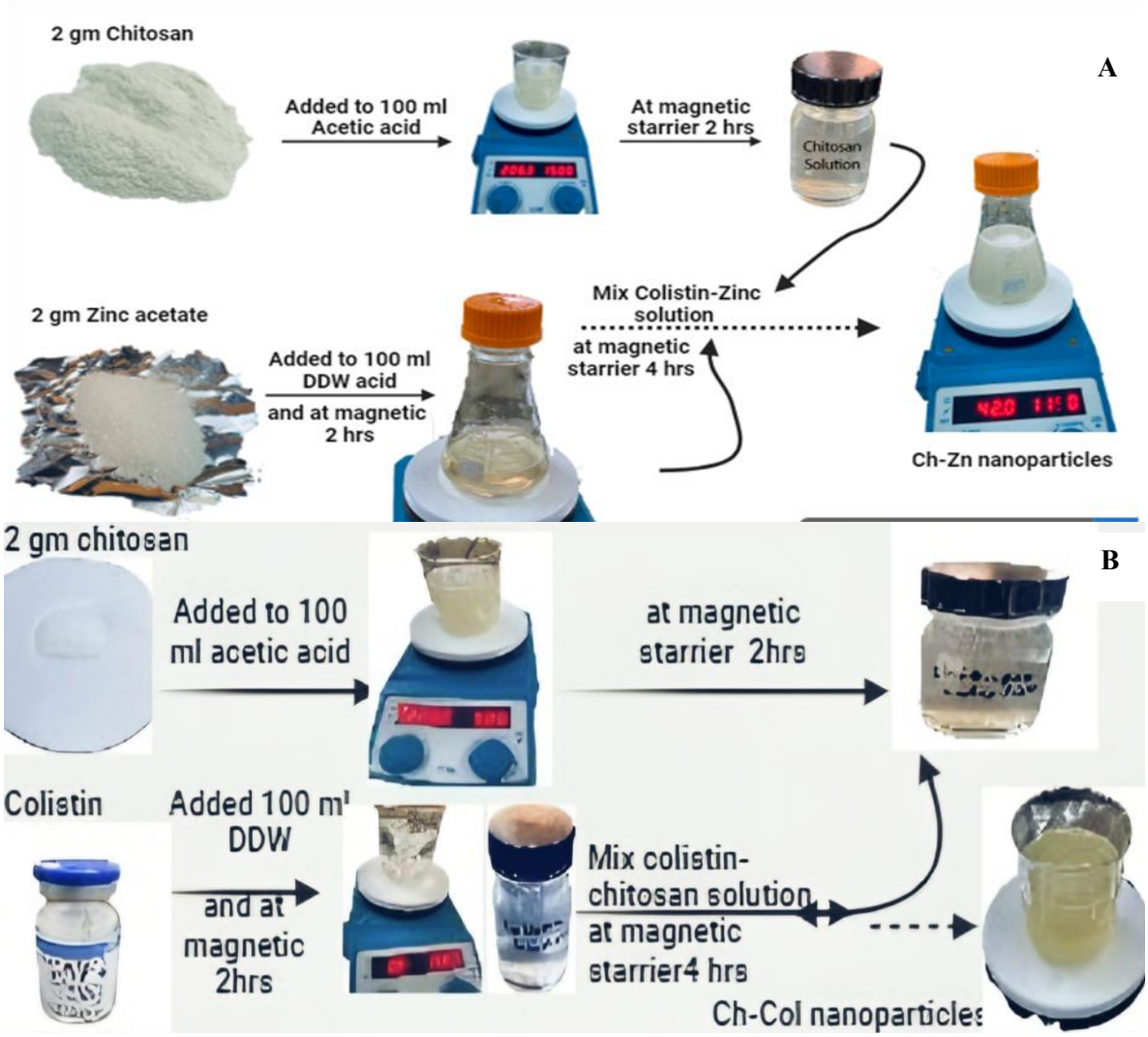

Fig 3. Schematic representation of synthesis steps: (a) Chitosan-ZnO nanoparticles (CS-ZnO NPs), and (b) Colistin-loaded chitosan nanoparticles (Col-CS-NPs).

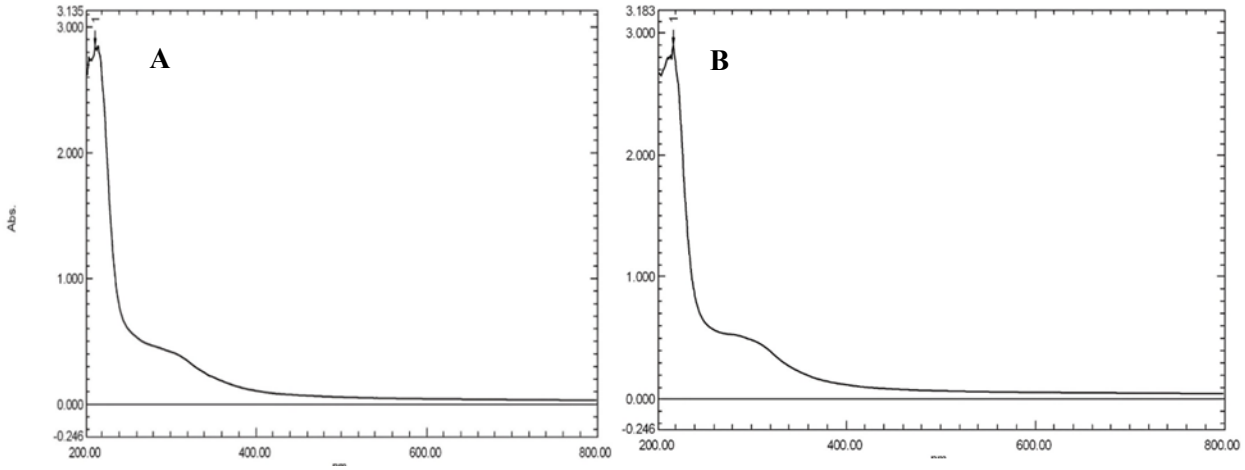

Fig 4. UV–Vis spectrophotometric analysis of biosynthesized nanoparticles: (a) CS-ZnO nanoparticles and (b) Col-CS nanoparticles, showing characteristic absorption peaks indicating successful synthesis.

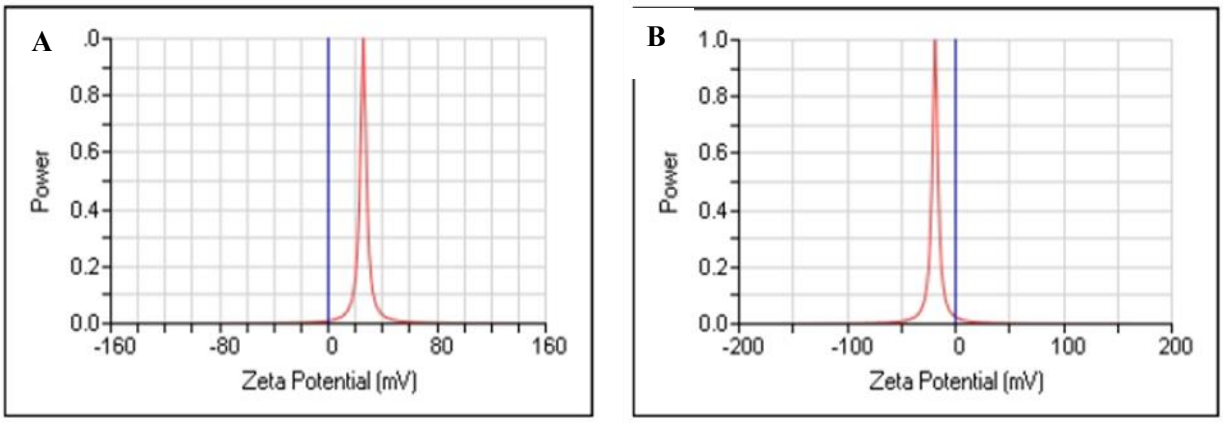

Fig 5. Zeta potential analysis of biosynthesized nanoparticles: (a) CS-ZnO nanoparticles showing near-neutral surface charge, and (b) Col-CS nanoparticles exhibiting strong negative surface charge, indicating enhanced colloidal stability.

According to the three-dimensional AFM, ZnO nanoparticles were discovered to have irregular and triangle cluster morphologies, ranging between 0.25 and 34.33 nm in height and 13 to 177 nm in diameter (as verified by a particle size analyzer) as seen in (Fig. 6-a).

Using the AFM, one may quantify the force at the nano-Newton scale exerted by the sample surface on the AFM tip and picture the nanoparticles in a three-dimensional surface profile with atomic resolution. To characterize their biosynthesis by analyzing nanoparticles produced through biological methods, focusing on their structure, size, distribution, and mechanical properties, which involves creating a three-dimensional surface profile, measuring nanoparticle size, and assessing their interaction forces to confirm the success and quality of the biosynthesis process, As seen in (Fig. 6-b), the study's result diameter indicated that the biosynthesized Col-CS NPs were 68 nm in diameter.

Field emission scanning electron microscope (FESEM) and transmission electron microscopy (TEM)

Utilizing scanning electron microscopy (SEM), the membrane's structural features and crystallinity were examined. An analysis was done to comprehend the NP samples' size, shape, and elemental and structural composition. CS-ZnO NP's spherical shape and diameter of 33nm are depicted in (Fig. 7-a) at a magnification of 13000x and 50000x. The chitosan nanoparticles used in the experiment took on the appearance of white powder.

Scanning electron micrographs of the Nanomagnetic chitosan revealed that they were about spherical. The groups of particles that make up the unaltered chitosan nanoparticles range from 10 to 33 nm. SEM images a specimen's surface using a concentrated, high-energy electron beam.

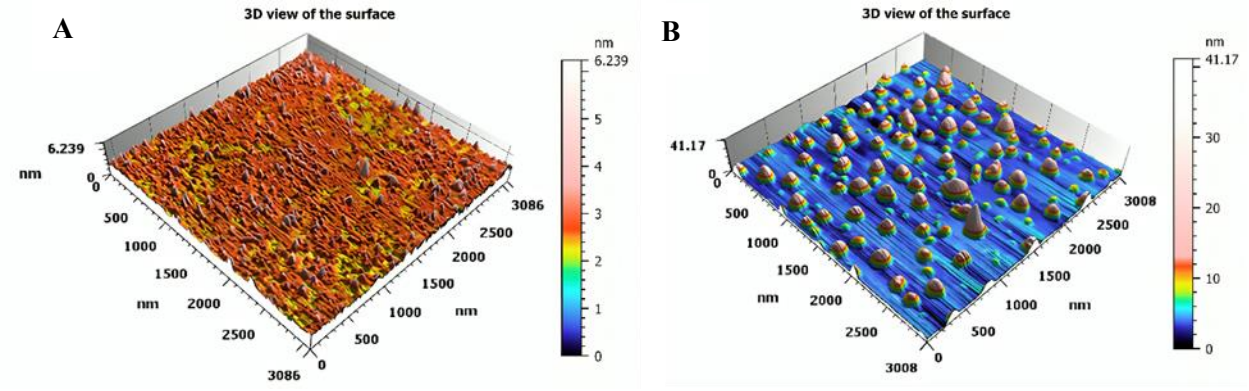

Fig 6. Atomic Force Microscopy (AFM) analysis of biosynthesized nanoparticles: (a) CS-ZnO nanoparticles and (b) Col-CS nanoparticles, illustrating surface morphology and particle size distribution.

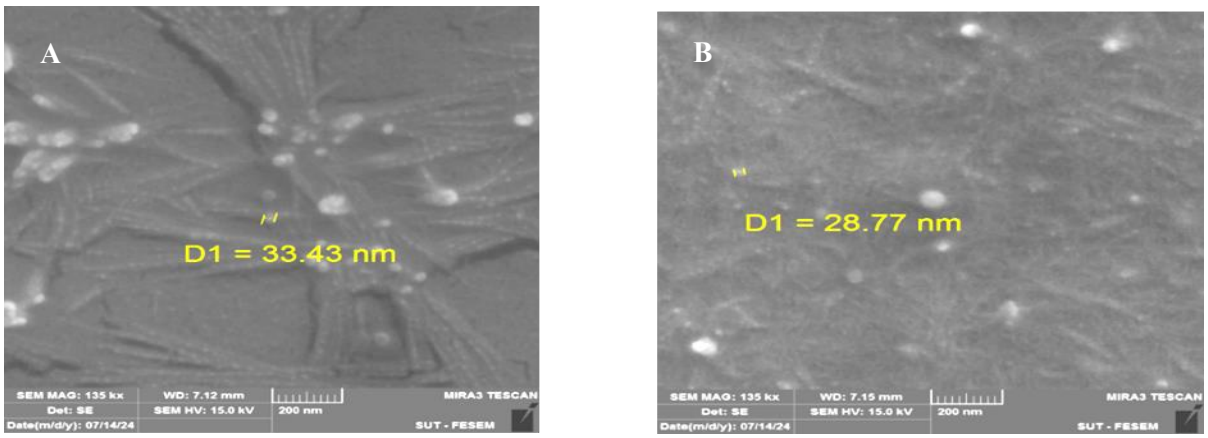

Fig 7. Field Emission Scanning Electron Microscopy (FESEM) images of biosynthesized nanoparticles: (a) CS-ZnO nanoparticles and (b) Col-CS nanoparticles, showing surface structure and morphology at high resolution.

SEM analysis determined the NP samples' size, morphology, elemental composition, and structural makeup. (Fig. 7-b) illustrates the spherical shape of Col-CS NPs with a diameter of 28nm through images captured at 3000 kv.

TEM can be used to investigate nanoparticles' size, shape, and degree of sphericality, as seen in (Fig. 8). A concentrated high-energy electron beam transmits the specimen in a TEM. The picture produced is visible on a phosphor screen or imaging system located on the other side of the impinging electron beam, Determining the morphology of CS-ZnO NPs and Col-CS NPs by analyzing the particles at 200 nm and 100 nm.

X-ray diffraction (XRD)

The XRD patterns showed that ZnO is crystalline and that ZnO-chitosan nanotechnology had low peak intensities, indicating that their crystallinity has decreased with a hexagonal quartzite structure. Because the sample pattern and the standard are nearly identical, it can be said that the wurtzite of CS-ZnO NPs is hexagonal and has nine significant peaks situated at (100), (002), (101), (102), (110), (103), (200), (112), and (201).

This research investigates the impact of chitosan modification on ZnO nanoparticles via the synthesis of ZnO/Chitosan using different molar ratios of Zn and CS, as shown in figure 9 a. with X-ray diffraction (XRD), one can investigate Col-CS-NP's kind and degree of crystallinity. X-ray diffraction (XRD) is the best analytical method for determining a material's crystalline phase or phases.

According to XRD examination (Fig 9 b), when chitosan forms CS-NPs through cross-linking with TPP, its distinctive broad peaks at $2\theta \approx 11°$ and 19.6° are essentially extinguished.

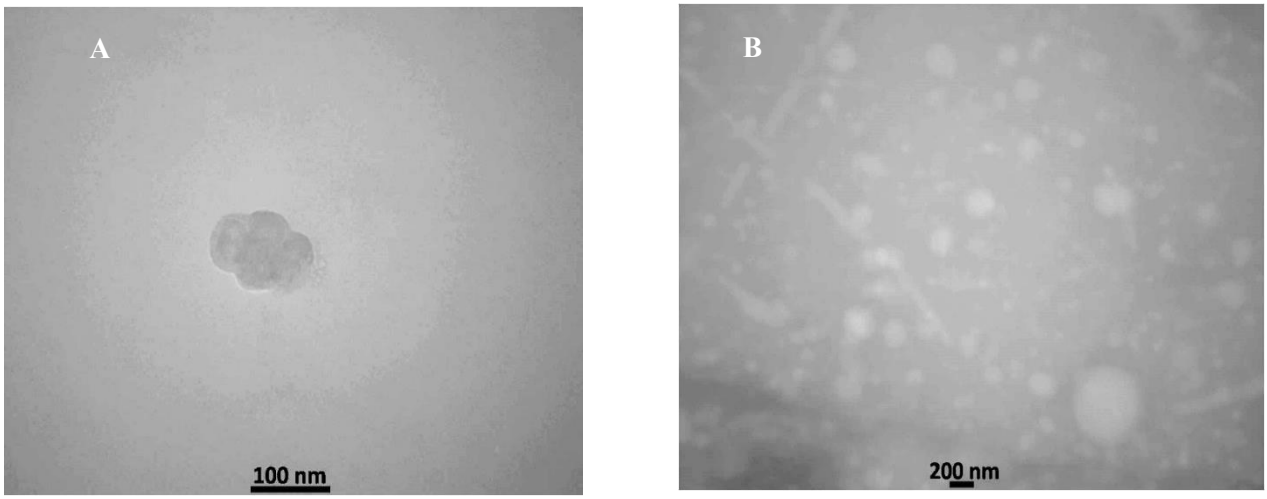

Fig 8. Transmission Electron Microscopy (TEM) images of biosynthesized nanoparticles: (a) CS-ZnO nanoparticles and (b) Col-CS nanoparticles, revealing detailed internal structure, shape, and size at the nanoscale level.

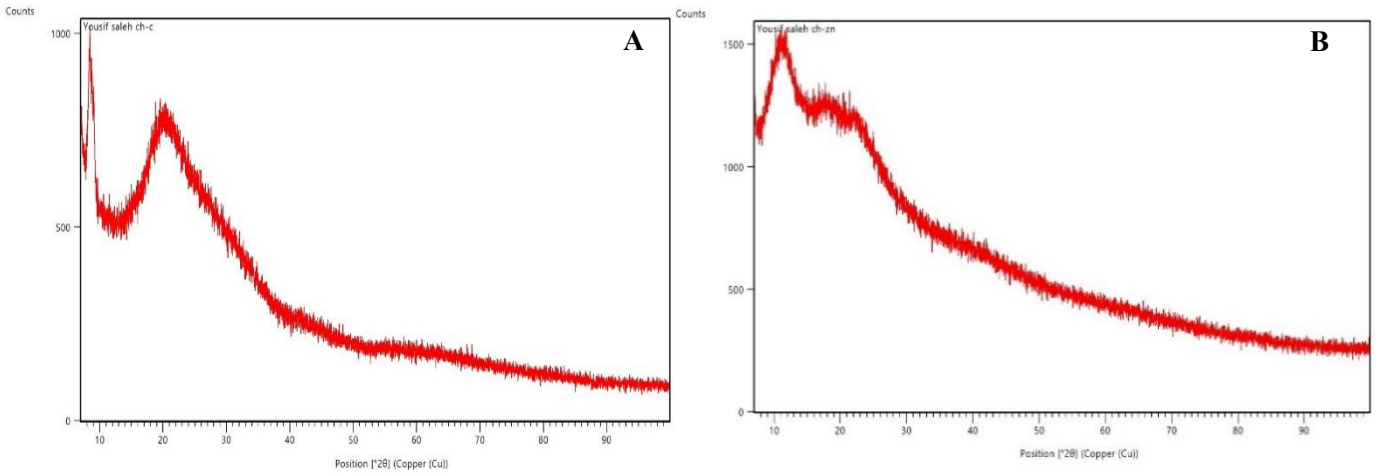

Fig 9. X-ray Diffraction (XRD) analysis of biosynthesized nanoparticles: (a) CS-ZnO nanoparticles and (b) Col-CS nanoparticles, demonstrating crystalline structure and phase identification.

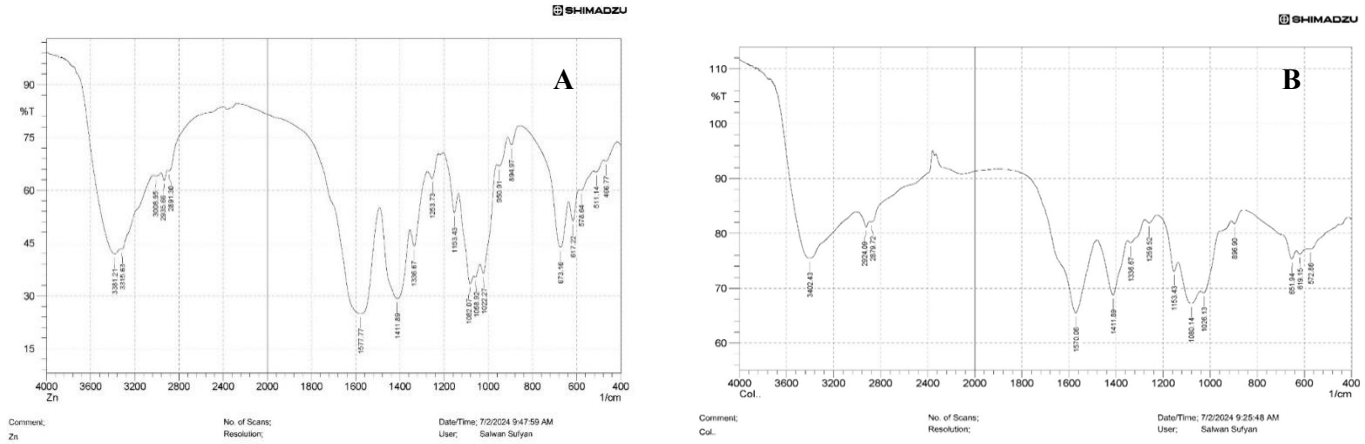

Fig 10. Fourier-transform infrared spectroscopy (FTIR) analysis of biosynthesized nanoparticles: (a) CS-ZnO nanoparticles and (b) Col-CS nanoparticles, illustrating characteristic functional groups and molecular interactions.

Fourier transform infrared (FTRI) analysis

The carbonyl group (-C=O) of chitosan and the C-H group of gelatins interact, as demonstrated by the hybrid composite films' FTIR spectra. Strong absorption can be detected at 3293 cm−1 (-OH stretching), 2925 cm−1 (N-H stretching of amide A), 1549 cm−1 (C-C, C stretching), 1410 cm−1 (C-O stretching), and 1640 cm−1 (C=O straining) in the FTIR spectra of the unaltered (CH/GL) specimen film as shown in (Fig. 10 a,b)

Energy dispersive X-ray (EDX)

ZnO nanoparticles have been identified within the polymer matrix of the CS/ZnO nanocomposite film, as shown by energy dispersive X-ray (EDX) examination in (Fig. 11-a). The EDX profile was conducted on the cylindrical particles on the coating in a single area.

The EDX analysis of CS-ZnO NPs shows C (35.5%), O (60.4%), and Zn (4.1%) according to table (4), confirming that ZnO nanoparticles are well-distributed within the CS matrix. The high Zn weight percentage (16.3%) highlights their significant contribution to the nanocomposite's properties.

Colistin chitosan nanoparticles (Col-CS-NPs) have been analyzed using energy dispersive X-ray (EDX) examination, as shown in the spectrum (Fig. 11-b). The

EDX profile was conducted on a single area of the particles on the coating, revealing their elemental composition.

The analysis shows C (53.4%) and O (33.7%) as the organic matrix's primary components. Additionally, minor elements such as Na (2.6%), Mg (0.5%), Si (8.6%), and Ca (1.2%) were detected, suggesting the presence of mineral or ionic species. The weight percentages (Table 5) highlight the significant contributions of C (41.6%), O (34.9%), and Si (15.7%), with smaller contributions from Na, Mg, and Ca, confirming the integration of these elements into the Col-CS-NPs matrix.

Antifungal properties of CS-ZnO NPs and Col-CS NPs

The MIC represents the lowest concentration of CS-ZnO NPs and Col-CS NPs required to prevent microbial growth. Owing to the challenges in MDI administration, the product concentrate was used instead of the MDI formulation, which was devoid of a propellant. The selenium nanoparticles significantly inhibited the growth of *Candida* species, as determined by the MIC method and the diameters of the inhibition zones.

In *Candida* species isolates tested, when compared *to Candida ferric and Candida albicans*, the antimicrobial activity of CS-ZnO NPs against *Candida guilliermondii* was generally higher, as shown in (Fig. 12-a). Additionally, it was demonstrated that, following treatment with Col-CS NPs at concentrations only between 1000 and 500 µg/mL, there was a significant difference ($p < 0.05$) in the dissemination mean zone of inhibition against *Candida albicans, Candida guilliermondii, and Candida ciferrii,* while other concentrations showed non-inhibition zone diameter according to (Fig. 12-b)

Determination of biofilm formation

Ten MDR isolates were tested for their biofilm production ability using a plastic microtiter plate. In Fig. 15, eight isolates were recorded as strong biofilm producers: Y2, Y5, Y1, Y4, Y3, Y8, Y10 and Y6 (20%, 19%, 19%, 14%, 10%, 8%, 6% and 6%), respectively, as detailed in (Fig. 14.) The biofilm formation of used isolates from patients can be seen in (Fig. 13).

Cytotoxic effect of CS/ZnONPs and Col-CS NPs nanocomposite

The cell line WRL 68 was initially thought to be derived from the embryonic liver. Cell lines used to measure the cytotoxic effect viability were reduced to half after treatment with the nanocomposite (298.2 and 19.29mg/L IC50), respectively; (Fig. 15-a-b) shows cell viability lowered with the nanocomposite concentration increment.

The cytotoxic effect of copper nanoparticles generally depends on the physicochemical properties, including particle shape, size, aggregation, crystallinity, and surface coating. A-375 is a *cell line* isolated from the skin of a patient with malignant *melanoma* cells used in this research that shows reduced viability after treatment with CS/ZnONPs and Col-CSNP nanoparticles in dose-dependent matter.

The IC50 nanocomposite values that inhibit cell line viability are 141.5 and 7.367 mg/l, respectively. According to the data collected by this test, cancer cell viability was much lower than that of WRL 68 cells in the same concentrations. This leads to the conclusion that CS/ZnONPs and Col-CSNPs nanocomposite significantly affected cancer cells

bap gene detection

Based on the MDR (multidrug resistance) of the isolates, ten *A. baumannii* isolates Y1-T15 with the *bap gene* were selected by the PCR results. The ethidium bromide-stained 1.5% agarose gel was electrophoresed at 75 volts for 50 minutes to confirm the positive gene result, and the result was visible under an ultraviolet (UV) transilluminator.

This investigation identified a distinct 184 of bp *bap gene* detection band respectively that was sharp, singular, and non-dispersed and that could be easily identified from the DNA ladder, as shown in (Fig. 16). Notably, the lack of any smearing of the gene band indicated that there was no evidence of DNA degradation the three isolations (Y3, Y4, and Y7) showed *bap gene* detection.

One of Col-CS NPs' main advantages is its ability to work against harmful microorganisms. Consequently, the ability of green synthesized Col-CS NPs to inhibit pathogenic Gram-negative bacteria was investigated.

The study examined the inhibitory effects of different dosages of NPs (1000–62.5 µg/mL), Table 6. Regarding Col-CS NPs, the Minimum Inhibitory Concentration (MIC) is the lowest concentration at which no growth is seen. According to the findings, the Col-CS NP minimum inhibitory concentration (MIC) for *A. baumannii* isolates was 500 µg/mL, and the sub-MIC was 250 µg/mL.

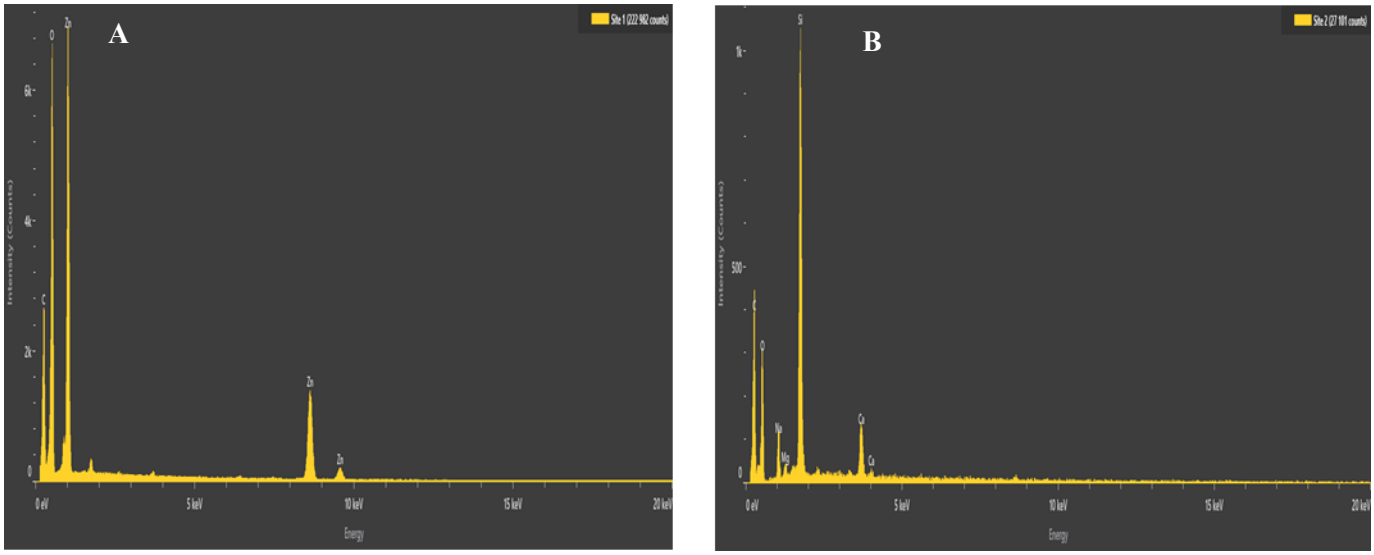

Fig 11. Energy-dispersive X-ray spectroscopy (EDX) analysis of biosynthesized nanoparticles: (a) CS-ZnO nanoparticles and (b) Col-CS nanoparticles, showing elemental composition and confirming the presence of key elements.

Table 4 Energy-dispersive X-ray spectroscopy (EDX) elemental composition of CS-ZnO nanoparticles, confirming the presence of key constituents.

Element	Atomic %	Atomic % Error	Weight %	Weight % Error
C	35.5	0.4	25.6	0.3
O	60.4	0.4	58.1	0.4
Zn	4.1	0.1	16.3	0.2

Table 5 Energy-dispersive X-ray spectroscopy (EDX) elemental composition of Col-CS nanoparticles, confirming the presence of essential elements

Element	Atomic %	Atomic % Error	Weight %	Weight % Error
C	53.4	1.2	41.6	0.9
O	33.7	0.9	34.9	0.9
Na	2.6	0.1	3.9	0.2
Mg	0.5	0.1	0.7	0.1
Si	8.6	0.1	15.7	0.2
Ca	1.2	0.1	3.1	0.1

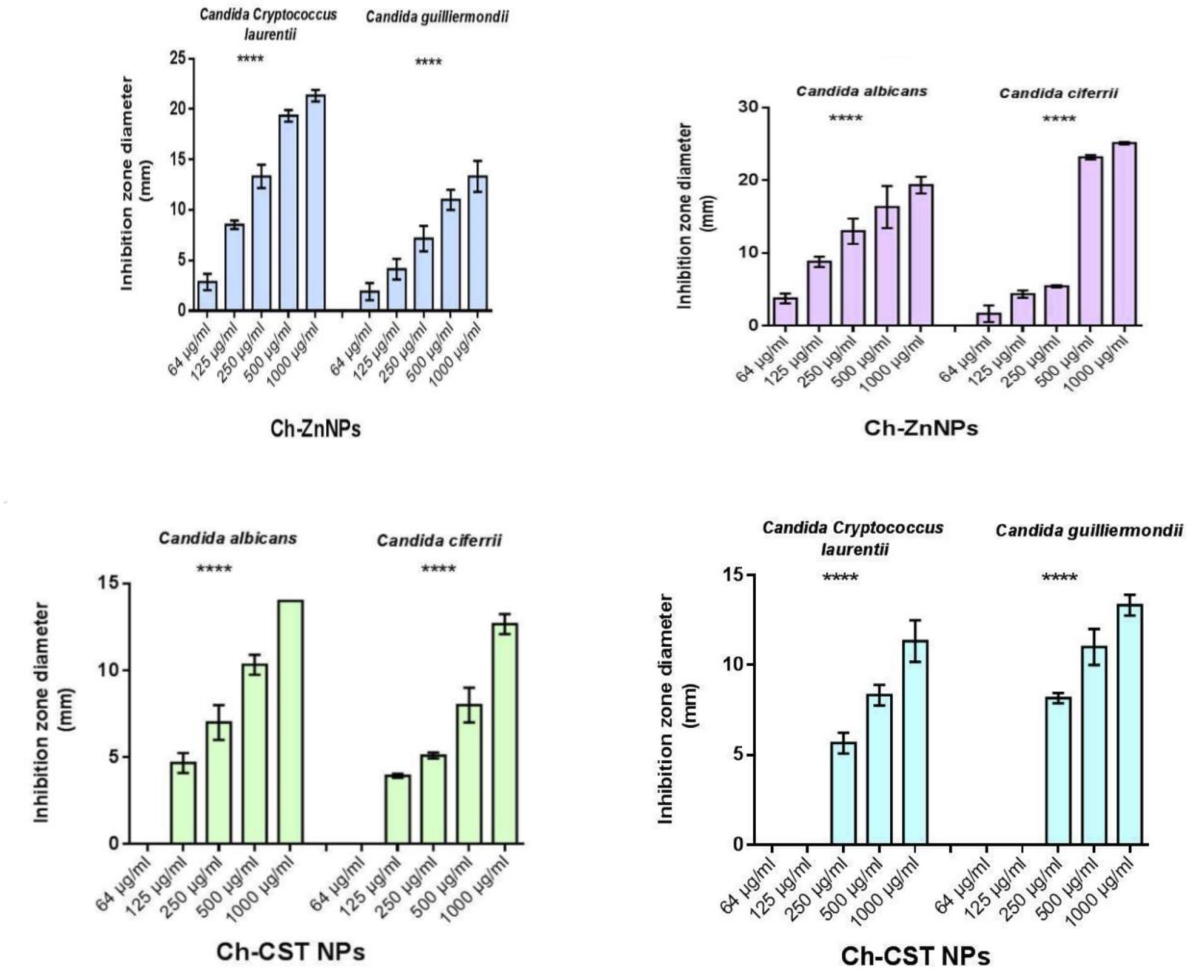

Fig 12. Mean ± SD Zone of Inhibition in mm treated with a) Col-CS NPs and b) Col-CS NPs against *Candida* spp at Different Concentrations between 1000, 500, 250, 125, and 62.5µg/mL.: Standard Deviation, (n = 3).

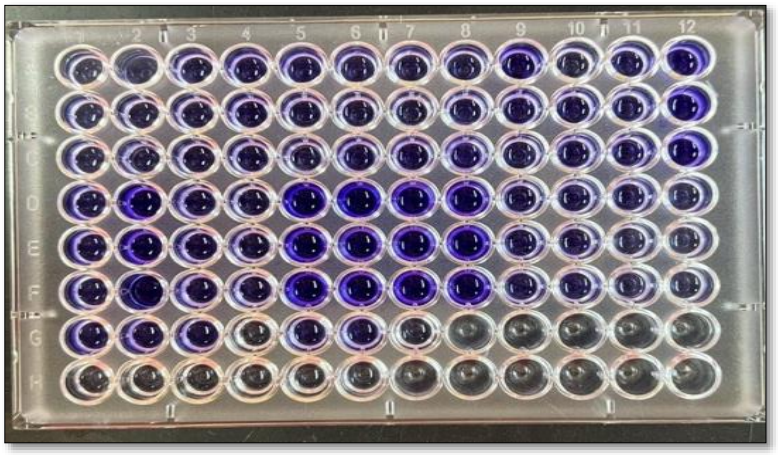

Fig 13. Microtiter plate assay for biofilm production by *Acinetobacter baumannii* isolates, demonstrating varying levels of adherence and biofilm-forming capacity.

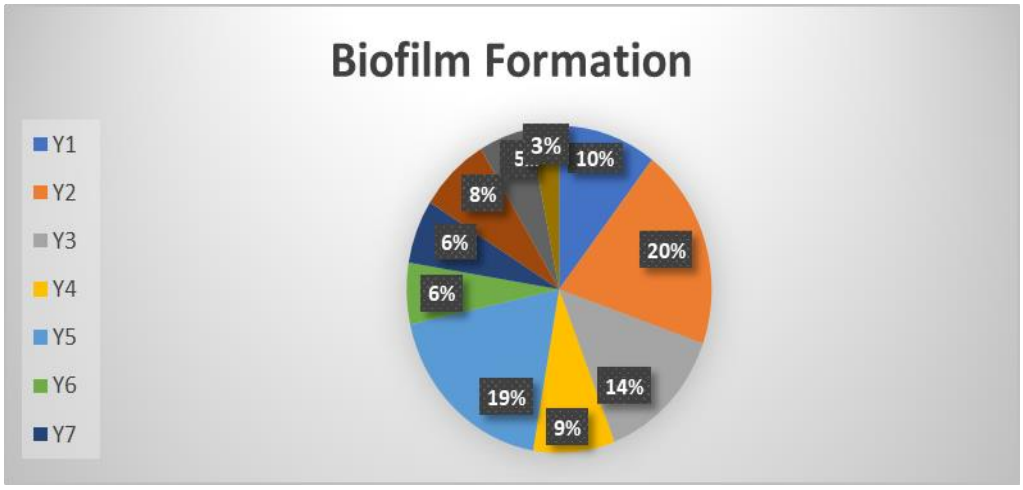

Fig 14. Percentage of biofilm formation by *Acinetobacter baumannii* isolates, indicating the extent of biofilm-producing capability among tested strains.

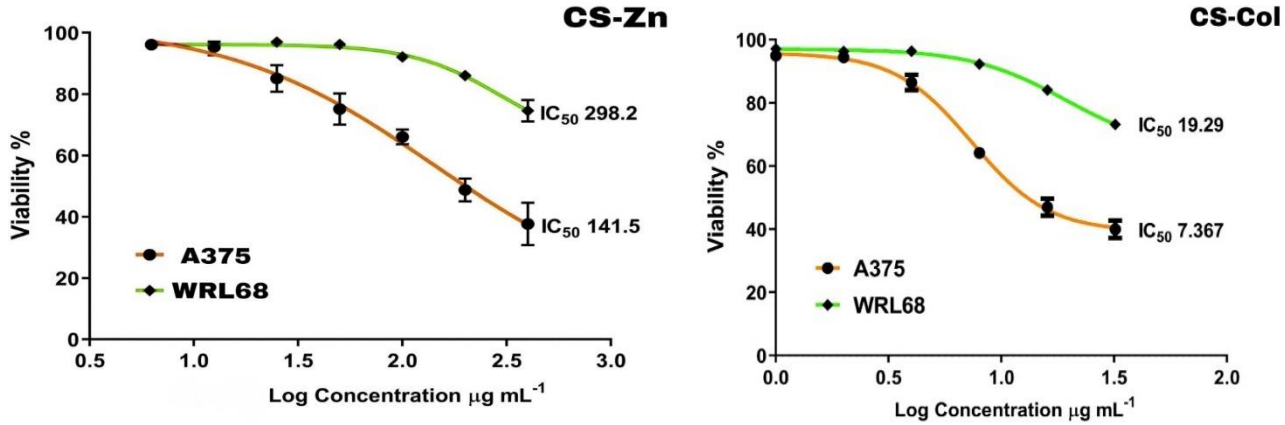

Fig 15. Cytotoxic effect of (a) CS/ZnO nanoparticles and (b) Col-CS nanoparticles on target cells, demonstrating dose-dependent viability responses.

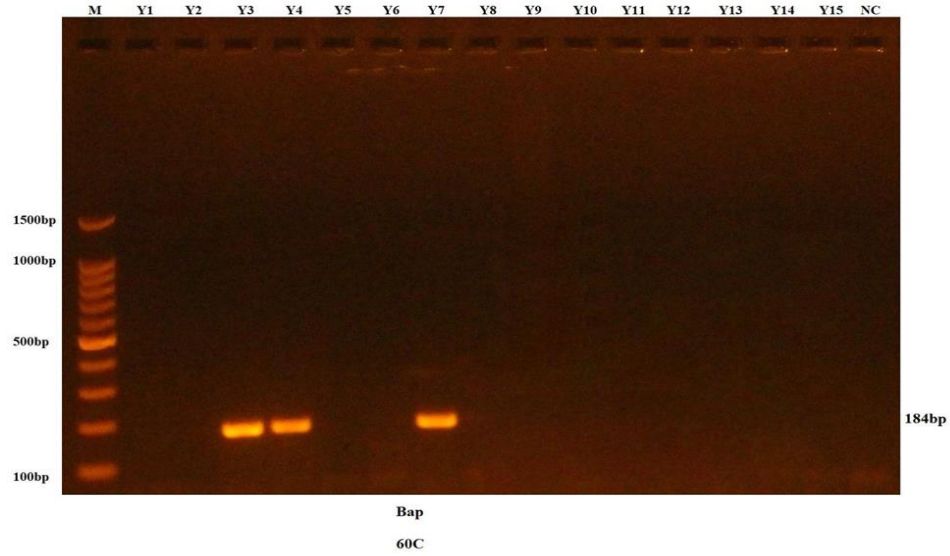

Fig 16. The amplification of *Bap genes* of bacterial species was fractionated on 1.5% agarose gel electrophoresis stained with Eth. Br. M: 100bp ladder marker. Lanes Y1-Y15 resemble 184bp PCR products

Table 6 Gene expression changes before and after chitosan-zinc nanoparticles

Sample	Acba-16s	*Bap*	DCT	DDCT	Folding
Y3 (before)	14.03	17.57	3.54	0.00	1.00
Y3 (after)	20.79	20.93	0.13	-0.40	0.59
Y4 (before)	17.17	18.09	0.92	0.00	1.00
Y4 (after)	20.34	20.47	0.13	-0.79	1.72
Y7 (before)	17.39	14.14	-3.25	0.00	1.00
Y7 (after)	20.25	20.33	0.07	3.32	0.10

Table 7 Gene **exp**ression changes before and after colistin-chitosan nanoparticles

Sample	Acba-16s	*Bap*	DCT	DDCT	Folding
Y3 (before)	14.03	17.57	3.54	0.00	1.00
Y3 (after)	19.50	19.98	0.48	-0.46	0.35
Y4 (before)	17.17	18.09	0.92	0.00	1.00
Y4 (after)	14.02	14.47	0.45	-0.47	1.38
Y7 (before)	17.39	14.14	-3.25	0.00	1.00
Y7 (after)	14.02	14.47	0.45	-0.47	1.38

Gene expression of Bap genes

RT-PCR reveals a significant downregulation in *Bap* expression after exposure to CS-ZnO-NPs suspension compared to regular gene expression in bacterial broth with no NPs involved. Fold change in gene expression reveals that *Bap* was downregulated in response to CS-ZnO-NPs in three isolates of *A. baumannii,* and the Y4 isolates were almost unaffected, as entailed in Table 6.

Fold change in gene expression reveals that *Bap* was downregulated in response to CS-ZnO-NPs in two out of three *Acinetobacter baumannii* isolates, but one isolate was unaffected. This could be due to the development of bacterial resistance mechanisms to nanoparticles.

Recent studies entailed several possible mechanisms bacteria use to overcome nanoparticles' effect, especially by the expression of genes responsible for producing biofilm components such as exopolysaccharides and developing resistance after many cultures' steps.

Three *A. baumannii* isolates were studied using the RT-qPCR technique to estimate the effect of synthesized colistin-chitosan nanoparticles. RT-PCR reveals in one isolate a significant decrease in ***Bap gene*** expression following the exposure to Col-CS-NPs compared to regular gene expression in bacteria.

In contrast, when exposed to Col-CS-NPs, *Bap* gene expression is significantly up-regulated. According to (Table 7), fold change in gene expression indicates that in two isolates, Y4 and Y7 *A. baumannii*, *Bap* genes were up-regulated; in another isolate, Y3, it was down-regulated in response to Col-CS-NPs.

Discussion

The antimicrobial activity of CS-ZnO-NPs can be attributed to their minute particle size, which facilitates penetration into bacterial membranes and subsequent cell destruction. Studies have demonstrated the anti-biofilm activity of nanoparticles, showing a concentration-dependent reduction in biofilm formation across various microorganisms (Laverde-Rojas et al., 2021).

Colistin is a re-emergent peptide antibiotic used as a last resort against multidrug-resistant (MDR) Gram-negative bacterial infections in clinical practice. However, the increasing prevalence of colistin-resistant bacteria poses a significant global public health concern. Nanotechnology-based approaches have shown promise in mitigating antibiotic resistance (Laverde-Rojas et al., 2021).

In agreement with (Türemen et al., 2021), UV-Vis spectra of chitosan, ZnO nanoparticles, and CS-ZnO nanocomposites revealed a blue shift in chitosan-coated samples, with zinc nanoparticle absorption peaks observed at 370 nm. AFM analysis confirmed that dried ZnO nanoparticles measured approximately 30 nm in size. These nanoparticles exhibited significant aggregation tendencies in hydrated states, as evidenced by pH-dependent size variations, zeta potential, and hydrodynamic diameter studies (Faiq & Ahmed, 2024). SEM imaging further demonstrated the successful production of chitin nanofibers from dietary sources like Alaskan pink shrimp and Japanese tiger prawns through a standardized process (Yousef et al., 2024).

The antimicrobial efficacy of CS-ZnO-NPs was supported by the observed reduction in minimum inhibitory concentration (MIC) values. This effect may be

due to chitosan's ability to destabilize bacterial membranes, enabling colistin (CST) to displace divalent cations (Ca2+ and Mg2+) from the lipopolysaccharide (LPS) layer. This displacement increases membrane fluidity and permeability, ultimately releasing cytoplasmic content and cell death (Ciro et al., 2019; Ahmed & Abdul Muhsin, 2024). Additionally, CST's interaction with negatively charged bacterial membranes, facilitated by electrostatic interactions, further enhances antimicrobial activity.

The structural integrity and purity of CS-ZnO-NPs were confirmed by diffraction peaks that matched ZnO and chitosan, indicating that ZnO's crystal structure remained intact upon bonding with chitosan (Ahmed & Abdul Muhsin, 2020). EDX analysis corroborated these findings, confirming the presence of zinc and oxygen as the sole elements in ZnO-CS nanomaterials. Nanoparticles can disrupt microbial components, including extracellular DNA (eDNA), crucial in bacterial adhesion, biofilm formation, and quorum sensing. The inhibition of peptides and proteins essential for biofilm and planktonic cell membranes makes them primary targets for current antimicrobial therapies (Ahmed et al., 2018).

Discrepancies between particle sizes observed via DLS and SEM were noted, as DLS measures the hydrodynamic diameter, which includes the particle core and surrounding shell. This shell comprises ligands, ions, and solvated water molecules, contributing to the larger sizes observed in aqueous media (Mahdi et al., 2024). In clinical contexts, the pathogenicity of *A. baumannii* is significantly influenced by its ability to form biofilms on various substrates, including those associated with ventilator-associated pneumonia and catheter-associated urinary tract infections (Azizi et al., 2016). Variations in *bap* gene expression levels were observed across clinical specimens, with the highest expression found in wound samples. This finding aligns with the role of biofilms in wound infections (Eijkelkamp et al., 2011).

Microdilution broth testing demonstrated the antibacterial activity of chitosan, AgNPs, and their antibiotic combinations, highlighting anti-efflux pump activity against *A. baumannii* and P. aeruginosa. Medium molecular weight chitosan and AgNPs showed significant synergistic effects (Kermanian et al., 2024). In iron-limited conditions, relative quantitative real-time PCR (rqRT-PCR) revealed *bap* expression variations, further supporting biofilms' role in bacterial survival (Rafei et al., 2022).

CS-ZnO-NPs composites exhibited superior inhibitory effects against Gram-positive, Gram-negative, and fungi, attributed to their antibiofilm properties and ability to reduce MIC values (Alharbi et al., 2023). Their anti-cancer potential has also been explored, with apoptosis identified as the primary mechanism of cell death induced by metal-based nanoparticles, followed by necrosis and autophagy. Autophagy activation leads to the breakdown of cellular components, offering an additional pathway for nanoparticle-induced cytotoxicity (Faiq & Ahmed, 2024).

Research into copper toxicity has highlighted its association with neurological disorders such as Alzheimer's disease, categorized under copper intolerance. Interactions between nanoparticles and biological systems can lead to oxidative stress, tissue inflammation, and histopathological changes (Kadhim et al., 2023).

Reactive oxygen species (ROS) generated by nanoparticles under oxidative stress can damage bacterial mitochondria and reduce membrane potential, thereby targeting bacterial cell membranes. These findings emphasize the multifaceted mechanisms by which nanoparticles exert their antimicrobial effects, with significant implications for combating multidrug-resistant pathogens and advancing therapeutic applications.

Conclusions

Thus, our in vitro study is designed to formulate and characterize experiments containing CS-ZnO nanoparticles (CS-ZnO NPs) and investigate their antimicrobial effects on both planktonic and biofilm forms of *A. baumannii*. The microbial load was reduced because of the synergistic effect between chitosan and ZnO nanoparticles. This work aims to develop a type of nano coating that multidrug-resistant bacteria may utilize in their reduced biofilm. It contains biological biopolymer chitosan and inorganic nanostructured materials ZnO. These metal oxides have some limitations when utilized in manufactured nanocomposites, primarily used in medication delivery and medical procedures, due to their increased toxicity at higher concentrations. The preceding results all suggest the necessity of more research to employ CS-ZnO NPs as potentially beneficial alternative antibacterial materials and in anti-cancer applications. Most pathogenic organisms we observed had the *bap* gene, frequently expressed in wound and chest sputum samples. Therefore, additional study is advised to determine how to prevent this gene's expression and the creation of biofilms, which will aid in treating illnesses brought on by *A. baumannii* strains that generate biofilms.

Conflict of Interest

The authors declare that they have no conflict of interest.

Funding

No governmental, commercial, or nonprofit funding agencies provided any funds for this project.

References

Abdel-Azeem A, Nada A, O'Donovan A, Thakur V K, Elkelish A. (2020). Mycogenic Silver Nanoparticles from Endophytic *Trichoderma atroviride* with Antimicrobial Activity. *Journal of Renewable Materials*, 8(2): 171-185

Abd-Elhameed A, Eladly A, Abdel-radi A, Mekky A. (2024). In vitro myco-synthesized copper oxide nanoparticles: A promising antiviral agent with antioxidant, anti-inflammatory, and anti-cancer activity. *Microbial Biosystems*, *9*(2), 195-207. doi: 10.21608/mb.2024.317736.1167

Abdulameer Kadhim AL-Ziadi S, Yass Lahmood W, Abd Alabbas Muhammad D, Rashid Swadi R. (2024). Bio-Production of silver nanoparticles by a Brevibacillus sp. and testing of its inhibitory efficacy on pathogenic fungi. Microbial Biosystems, 9(2), 58-66. doi: 10.21608/mb.2024.296842.1106

Ahmed M E, Abdul Muhsin Z A. (2020). Synergistic effect of gentamicin and silver nanoparticles against antibiotic-resistant *Pseudomonas aeruginosa* isolated from burns. *Al-Anbar Medical Journal*, 13(1), pp.73-80.

Ahmed M E, Abdul Muhsin Z A. (2024). Synergistic effect of gentamicin and iron oxide nanoparticles on *phzM* gene of *Pseudomonas aeruginosa*. *Microbiology Journal*, 3, pp.27–39. https://doi.org/10.15407/microbiolj86.03.027.

Ahmed M E, Kadhim A R. (2018). Effects of bacteriocin from MRSA and *Nigella sativa* (seed oil) against biofilm from MRSA. *International Journal of Pharmaceutical Quality Assurance*, 9(2), pp.199-203.

Ahmed M E (2018). The study of *Pseudomonas fluorescens* and *Citrus limon* bacteriocin effects against *Propionibacterium acnes* and *Staphylococcus epidermidis* in acne patients. *Journal of Physics: Conference Series*, 1003(1), p.012004. https://doi.org/10.1088/1742-6596/1003/1/012004.

Ahmed M E, Al-Awadi A Q, Abbas A F. (2023). Focus on synergistic bacteriocin-nanoparticles enhancing antimicrobial activity assay. *Microbiology Journal*, 6, pp.95-104. https://doi.org/10.15407/microbiolj85.06.095.

Ahmed M E, Khalaf Z Z, Ghafil J A, Al-Awadi A Q. (2018). Effects of silver nanoparticles on biofilms of *Streptococcus* spp. *Executive Edition*, 9, p.1216.

Ahmed M E, Sulaiman G M, Hasoon B A, Khan R A, Mohammed H A. (2024). Green synthesis and characterization of apple peel-derived selenium nanoparticles for anti-fungal activity and effects of MexA gene expression on efflux pumps in *Acinetobacter baumannii*. *Applied Organometallic Chemistry*, e7805.

Alharbi R A, Alminderej F M, Al-Harby N F, Elmehbad NY, Mohamed N A. (2023). Design, synthesize, and characterize novel bis-uracil chitosan hydrogels modified with zinc oxide nanoparticles to boost their antimicrobial activity. *Polymers*, 15(4), p.980. https://doi.org/10.3390/polym15040980.

Alnagar N, Hasanin M, Suleiman W, Zaki S, Hashem A. (2025). Preparation of nanocomposite based on zinc oxide nanoparticles and biopolymers: Characterization, antimicrobial and anticancer activities. *Microbial Biosystems*, 10(1), 68-81. doi: 10.21608/mb.2025.325211.1186

Azizi O, Shahcheraghi F, Salimizand H, Modarresi F, Shakibaie M R, Mansouri S. (2016). Molecular analysis and expression of *bap* gene in biofilm-forming multidrug-resistant *Acinetobacter baumannii*. *Reports of Biochemistry & Molecular Biology*, 5(1), pp.62-72.

Azizi O, Shahcheraghi F, Salimizand H, Modarresi F, Shakibaie M R, Mansouri S. (2016). Molecular analysis and expression of *bap* gene in biofilm-forming multidrug-resistant *Acinetobacter baumannii*. *Reports of Biochemistry & Molecular Biology*, 5(1), pp.62-72.

Bahador A, Saghii H, Ataee R, Esmaeili D. (2015). The study of inhibition effects of *Satureja khuzestaniea* essence against gene expression *bap* in *Acinetobacter baumannii* with real-time PCR technique. *Iranian Journal of Medical Microbiology*, 9(1), pp.42-49.

Changsan N, Atipairin A, Muenraya P, Sritharadol R, Srichana T, Balekar N. et al. (2024). In vitro, evaluation of colistin conjugated with chitosan-capped gold nanoparticles as a possible formulation applied in a metered-dose inhaler. *Antibiotics*, 13(7), p.630. https://doi.org/10.3390/antibiotics13070630.

Chukamnerd, A., Saipetch, N., Singkhamanan, K., Ingviya, N., Assanangkornchai, N., Surachat, K. et al. (2024). Association of biofilm formation, antimicrobial resistance, clinical characteristics, and outcomes among *Acinetobacter baumannii* isolates from patients with ventilator-associated pneumonia. *Clinical Respiratory Journal*, 18(1).

Ciro Y, Rojas J, Oñate-Garzon J, Salamanca C H. (2019). Synthesis, characterization, and biological evaluation of ampicillin-chitosan-polyanion nanoparticles produced by ionic gelation and polyelectrolyte complexation assisted by high-intensity sonication. *Polymers*, 11, p.1758.

Dil E A, Asfaram A, Goudarzi A, Zabihi E, Javadian H. (2020). Biocompatible chitosan-zinc oxide nanocomposite-based dispersive micro-solid phase

extraction coupled with HPLC-UV for determination of rosmarinic acid in extracts of medicinal plants and water samples. *International Journal of Biological Macromolecules*, 154, pp.528-537.

Divya K, Jisha M S. (2018). Chitosan nanoparticles: Preparation and applications. *Environmental Chemistry Letters*, 16, pp.101-112.

Eijkelkamp B A, Hassan K A, Paulsen I T, Brown M H. (2011). Investigation of the human pathogen *Acinetobacter baumannii* under iron-limiting conditions. *BMC Genomics*, 12, p.126. https://doi.org/10.1186/1471-2164-12-126.

Emad M, Salama K. (2020). A comparison of the effects of lemon peel-silver nanoparticles versus brand toothpastes and mouthwashes on *Staphylococcus* spp. Isolated from teeth caries. *Iraqi Journal of Science*, 61(8), pp.1894-1901. https://doi.org/10.24996/ijs.2020.61.8.6.

Faiq N H, Ahmed M E. (2024). Effect of biosynthesized zinc oxide nanoparticles on phenotypic and genotypic biofilm formation of *Proteus mirabilis*. *Baghdad Science Journal*, 21(3), 0894.

Fawzi F H, Ahmed M E. (2024). Green synthesis and characterization of selenium nanoparticles via *Staphylococcus warneri* approach: Antimicrobial effects on *PhzM* pyocyanin gene expression in *Pseudomonas aeruginosa*. *Plasmonics*. https://doi.org/10.1007/s11468-024-02378-2.

Fuster M G, Montalbán M G, Carissimi G, Lima B, Feresin G E, Cano M. et al. (2020). Antibacterial effect of chitosan-gold nanoparticles and computational modeling of the interaction between chitosan and a lipid bilayer model. *Nanomaterials*, 10, p.2340.

Gezaf S, Hamedo H, Ibrahim A, Mossa M. (2022). Mycosynthesis of silver nanoparticles by endophytic Fungi: Mechanism, characterization techniques and their applications. *Microbial Biosystems*, 7(2), 48- 65. doi: 10.21608/mb.2023.185718.1066

Hassan Z J S, Hamid M K, Ahmed M E. (2022). Synthesized zinc oxide nanoparticles were synthesized using the precipitation method on *Streptococcus* spp. from dental caries and cytotoxicity assay. *International Journal of Drug Delivery Technology*, 12, pp.1327-1330.

Hassoon H, Ahmed M, Qaddoori Y. (2019). Efficiency of silver nanoparticles against bacterial contaminants isolated from water in Basra. *The Eurasia Proceedings of Science Technology Engineering and Mathematics*, 7, pp.164-174.

Hussein R, Abdul Aziz F, Al-Haideri H, Al-Qaysi S. (2025). Novel biosynthesis of manganese dioxide nanoparticles using watermelon peel extract and their biological applications. *Microbial Biosystems*, 10(1), 112-122. doi: 10.21608/mb.2025.314779.1155

Jaber N, Al-Remawi M, Al-Akayleh F, Al-Muhtaseb N, Al-Adham I S I, Collier P J. (2022). A review of the antiviral activity of chitosan, including patented applications and its potential use against COVID-19. *Journal of Applied Microbiology*, 132, pp.41-58.

Kadhim, Z.H., Ahmed, M.E. and Şimşek, I., 2023. Biologically synthesized copper nanoparticles from *Staphylococcus epidermidis* on resistant *Staphylococcus aureus* and cytotoxic assay. *Bionatura*, 8(1).

Kermanian K, Farahpour M R, Tabatabaei Z G. (2024). Accelerative effects of alginate-chitosan/titanium oxide@geraniol nanosphere hydrogels on the healing process of wounds infected with *Acinetobacter baumannii* and *Streptococcus pyogenes* bacteria. *International Journal of Biological Macromolecules*, 254, p.127549.

Laverde-Rojas V, Liscano Y, Rivera-Sánchez S P, Ocampo-Ibáñez I D, Betancourt Y, Alhajj M J. (2021). Antimicrobial contribution of chitosan surface-modified nanoliposomes combined with colistin against sensitive and colistin-resistant clinical *Pseudomonas aeruginosa*. *Pharmaceutics*, 13(1), p.41. https://doi.org/10.3390/pharmaceutics13010041.

Mahdi M S, Fadhil A A, Ahmed M E. (2024). Cytotoxicity of zinc oxide nanoparticles to lymphocytes using *Enterococcus faecium* bacteriocin and assessment of their antibacterial effects. *Nanomedicine Research Journal*, 9(2), pp.180-194. https://doi.org/10.22034/nmrj.2024.02.007.

Mahdi S M , Ahmed M E, Abbas A F. (2024). Effect of enterococci–zinc oxide nanoparticles on gene expression of *rsbA* swarming genes in *Proteus mirabilis* isolated from catheter urine. *Biomedicine and Pharmacotherapy Journal*, 17(2). https://bit.ly/44Rv7Ec.

Mahdi S M, Ahmed M E, Abbas A F. (2024). Effect of enterococci–zinc oxide nanoparticles on gene expression of *rsbA* swarming genes in *Proteus mirabilis* isolated from catheter urine. *Biomedicine and Pharmacotherapy Journal*, 17(2). https://bit.ly/44Rv7Ec.

Mossa M, Gezaf S, Ibrahim A, Hamedo H. (2024). Preliminary screening of endophytic fungi hosted some wild plants in North Sinai for biogenic production of silver nanoparticles. *Microbial Biosystems*, 8(2), 57-73. doi: 10.21608/mb.2024.341385

Muunim H H, Al-Mossawei M T, Ahmed M E. (2019). Comparative study among MRSAcin, Nisin A, and vancomycin on biofilm formation by methicillin-resistant *Staphylococcus aureus* isolated from food sources. *International Journal of Drug Delivery Technology*, 39(3), pp.176-181.

Passat D N F. (2016). A local study of blaCTX-M gene detection in Proteus spp. was conducted using the PCR technique. *Iraqi Journal of Science*, pp.1371–1376. https://ijs.uobaghdad.edu.iq/index.php/eijs/article/view/7107.

Rafei R, Koong J, Osman M, Al Atrouni A, Hamze M, Hamidian M. (2022). Analysis of *pCl107*, a large plasmid carried by an ST25 *Acinetobacter baumannii* strain, reveals a complex evolutionary history and links to multiple antibiotic resistance and metabolic pathways. *FEMS Microbes*, 3.

Rasheed A E, Hamid M K, Ahmed M E. (2023). A green synthesis of zinc oxide nanoparticles against MRSA wound healing in vivo. *Journal of Nanostructures*, 13(4), pp.989-998. https://doi.org/10.22052/JNS.2023.04.008.

Rashid A E, Ahmed M E, Hamid M K. (2022). Evaluation of antibacterial and cytotoxicity properties of zinc oxide nanoparticles synthesized by precipitation method against methicillin-resistant *Staphylococcus aureus*. *International Journal of Drug Delivery Technology*, 12(3), pp.985-989.

Romi Z M, Ahmed M E. (2024). The influence of biologically synthesized copper nanoparticles on the biofilm produced by *Staphylococcus haemolyticus* isolated from seminal fluid. *Iraqi Journal of Science*, pp.1948-1968.

Salah Y, Moza M, Abdel-Azeem A M. (2025). Mycogenic synthesis of different nanoparticles by endophytic fungi hosted higher plants. *Microbial Biosystems*, 10(1), 243-254. doi: 10.21608/mb.2025.414972

Salman M F, Ahmed M E A. (2024). The effect of selenium nanoparticles on the expression of the *MexB* gene of *Pseudomonas aeruginosa* isolated from wound and burn infections. *Iraqi Journal of Medical Sciences*, 22(1), pp.79-92. https://doi.org/10.22578/IJMS.22(10).

Seddiq S H, Zyara A M, Ahmed M E. (2023). Evaluation of the antimicrobial action of kiwifruit zinc oxide nanoparticles against *Staphylococcus aureus* isolated from cosmetics tools. *BioNanoScience*. https://doi.org/10.1007/s12668-023-01142-.

Srivastava S, Usmani Z, Atanasov AG, Singh VK, Singh NP, Abdel-Azeem AM, Prasad R, Gupta G, Sharma M, Bhargava A. (2021). Biological Nanofactories: Using Living Forms for Metal Nanoparticle Synthesis. *MiniReviews in Medicinal Chemistry*, 21, 245-265

Türemen M, Demir A, Gokce Y. (2021). The synthesis and application of chitosan-coated ZnO nanorods for multifunctional cotton fabrics. *Materials Chemistry and Physics*, 268, p.124736.

Yousef N S, Shokry F, Elkhatib M. (2024). Chitosan/PVA nanofibers and membranes: Preparation, characterization, and potential applications. *Port-Said Engineering Research Journal*, 28(1), pp.103-111.